Corrosion behaviour of Cu–2Ti and Cu–2Zr (wt%) alloys in neutral aerated sodium chloride solution

Corrosion behaviour of Cu-2Ti and Cu-2Zr (*wt.* %) alloys in neutral aerated sodium chloride solution

F. Rosalbino*, G. Scavino

Dipartimento di Scienza Applicata e Tecnologia (DISAT), Politecnico di Torino

Corso Duca degli Abruzzi 24, I-10129 Torino (Italy)

D. Macciò

Dipartimento di Chimica e Chimica Industriale, Università di Genova

Via Dodecaneso 31, I-16146 Genova (Italy)

Abstract

The corrosion behaviour of Cu-2Ti and Cu-2Zr (*wt.* %) alloys has been assessed by open circuit potential and electrochemical impedance spectroscopy (EIS) measurements carried out in 3.5 *wt.*% NaCl solution, at approximately neutral pH, without stirring and in contact with the air. For comparison, the electrochemical tests have also been carried out on unalloyed Cu. Electrochemical impedance results showed that Ti and Zr alloying additions significantly increase the corrosion resistance of copper, the best behaviour being observed for the Cu-2Zr alloy. This improvement may be ascribed to the formation of Ti- or Zr-enriched passive layer which exhibits higher protective effectiveness compared with that of unalloyed Cu.

Keywords*:* Copper; Alloying elements; Corrosion behaviour; Sodium chloride solution; Electrochemical Impedance Spectroscopy (EIS)

* Corresponding author. Tel.: +39-011-0904760; fax: +39-011-0904699

E-mail address: francesco.rosalbino@polito.it (F.Rosalbino)

1. Introduction

Age-hardenable Cu-Ti and Cu-Zr alloys containing approximately 1 – 5 mass% Ti or Zr are receiving a great deal of attention as ultra-high strength conductive materials for extensive applications such as overhead contact wires for electric railway, electrodes and holders for welding, electrical components working under mechanical stress and spark, lead frame for integrated circuits, moulds and dies for continuous casting metals, heat sinks for nuclear power reactors, etc., essentially replacing the conventional expensive and toxic Cu-Be alloys [1]. Their advantages include excellent electrical and thermal conductivities, ease of fabrication, high fatigue resistance and radiation resistance, and low toxicity. Through age-hardening, the mechanical and tribological properties of the alloys can be enhanced while high levels of electrical conductivity can be preserved [1]. The applications of Cu-Ti and Cu-Zr alloys may involve acidic, alkaline and chloride-containing environments. Although copper is a noble metal, it reacts readily in oxygen-containing environment, with the anodic dissolution of copper electrochemically balanced by oxygen reduction [2, 3]. Considering the widespread use of Cu-Ti and Cu-Zr alloys, their corrosion behaviour in adverse working conditions is critical for determining the lifetime and reliability of the engineering components.

A few authors studied the influence of chloride-containing environments on the corrosion properties of Cu-Ti and Cu-Zr alloys. Wei and his coworkers reported the effect of artificial ageing on the corrosion behaviour of Cu-4 *wt.*% Ti alloys in 3.5 *wt.*% NaCl solution [4]. Corrosion tests showed that ageing treatment changed the corrosion morphology of the alloys. All specimens were susceptible to both intergranular and pitting corrosion. The pitting corrosion susceptibility decreased with increasing ageing time. Lu and his coworkers studied the corrosion behaviour of Cu-Zr alloys with 15%, 30% and 68% of Zr in 0.1 M HCl [5], The results revealed that Cu-15%Zr had the highest corrosion resistance in the potential region of selective dissolution of Zr while the Zr content had little effect on the selective dissolution rate of Zr when it was above 30%. However, the corrosion properties of high copper alloys low-alloyed with Ti and Zr in chloride-containing environments have not been investigated extensively.

In this study we compared the corrosion behaviour of Cu-2Ti and Cu-2Zr (*wt.* %) alloys with the behaviour displayed by unalloyed copper in order to gain information about the influence of titanium and zirconium on corrosion process. The corrosion behaviour was assessed by recording the open circuit potential as a function of time in neutral aerated sodium chloride solution, and by electrochemical impedance spectroscopy (EIS).

2. Experimental

The metals used were Cu, Ti, Zr (99.99 *wt.*%, nominal purity) all from NewMet Koch, Waltham Abbey, UK. The Cu-2Ti and Cu-2Zr (*wt.*%) alloys, with a mass of about 3 g, were prepared from small pieces of the elements, previously cleaned by filing, and melted in arc furnace under argon atmosphere to prevent oxidation. Homogeneity was assured by repeated melting and reversing. Moreover, the alloys were sealed in quartz vials under argon atmosphere, and annealed at 700°C for 24 h, later at 500°C, for two days. Finally, they were let cooling in the furnace switched off.

Microstructural characterization of the alloys prior the electrochemical tests was carried out by means of Light Optical Microscopy (LOM) and Scanning Electron Microscopy (SEM), Zeiss model EVO 40, coupled with Electron Microprobe Analysis (EPMA), Oxford Instruments model Tetralink Pentafet. The metallographic samples were prepared and dry-polished by standard methods, with polycrystalline diamond up to 1 μm.

Electrochemical experiments were conducted at 25 ± 1 °C in a standard three-electrode cell with 0.5 cm^2 of exposed area in the working electrode, having a platinum mesh as counter electrode and a saturated calomel electrode (SCE) as reference. The working electrolyte was a naturally aerated 3.5 *wt.*% NaCl solution (pH = 6.5). Before each measurement, the samples surface was first ground with 320, 400 and 600 μm SiC abrasive papers in anhydrous ethyl alcohol and then automatically polished up to 1 μm using diamond pastes and non aqueous lubricants until a mirror-bright surface was achieved.

Open circuit potential, E_{OC}, measurements were carried out on freshly polished samples, in naturally aerated aqueous electrolyte without stirring, immediately after polishing. The E_{OC} was continuously monitored during 1 h exposure.

Electrochemical impedance was measured at the open circuit potential using a Gamry FAS2 Femtostat with a PC4 Controller. The frequency range analyzed went from 100 kHz up to 10 mHz, with the frequency values spaced logarithmically (seven per decade). The width of the sinusoidal voltage signal applied to the system was 10 mV rms (root-mean-square). Impedance measurements were performed at different exposure times in the electrolyte.

For comparison, the electrochemical tests were also performed on unalloyed Cu supplied by Johnson Matthey, London, UK.

SEM-EPMA were used to investigate morphology and chemical composition of alloys surfaces after the electrochemical tests.

3. Results and discussion

The alloys present a micrographic aspect corresponding essentially to equilibrium condition, due to the annealing they have been subjected to obtain homogenisation. Both Cu-2Ti and Cu-2Zr alloys show a two-phase morphology characterized by a Cu-based matrix, containing up to 0.1 *wt.*% alloying element, and a Cu-rich intermetallic phase. Results of the SEM-EPMA characterization are listed in Table 1. Phase compositions are values averaged on several quantitative measurements on different spots. Optical micrographs representative of the studied alloys are reported in Figures 1 and 2.

Figure 3 shows the open circuit potential, E_{OC}, as a function of time for unalloyed Cu and Cu-2M (M = Ti, Zr) alloys in quiescent 3.5 *wt.*% NaCl aerated solution. The E_{OC} curve of unalloyed Cu shows a negative shift at a steady state potential of approximately −210 mV(SCE) while Cu-2Ti and Cu-2Zr alloys have a negative shift with a steady state potential of −310 mV(SCE) and −280 mV(SCE), respectively. The E_{OC} of unalloyed Cu and Cu-2M alloys was decreased immediately after exposure to the aggressive environment. This indicates the breakdown of the spontaneous air-

formed oxide film and exposing the underlying surface. In all cases, the steady state potential was reached within 360 s from electrode exposure to NaCl solution, and results in the gradual formation of stable passive layers on the surface.

Figure 4 shows the evolution of the impedance diagrams, in the form of Nyquist plots, for unalloyed Cu, as a function of exposure time to aerated 3.5 *wt.*% NaCl solution. Some curves were omitted to keep the figure clear. The impedance spectra are characterized by two capacitive loops which are not well defined. The time constant at high frequencies is attributed to the passive layer while the second at the intermediate and low frequencies to the faradaic charge transfer process. Several authors have found similar results for copper in chloride-containing solutions [6 - 8]. The increase of impedance values with increase of exposure time implies that the passive layer becomes more protective for exposure time up to 168 h.

Figure 5 shows the evolution of impedance diagrams, in the form of Nyquist plots, for Cu-2M alloys as a function of exposure time to aerated 3.5 *wt*.% NaCl solution. The impedance of Cu-2Ti and Cu-2Zr alloys displays similar features to that of unalloyed Cu, i.e. two not well defined capacitive loops at high and low frequencies. Compared with unalloyed Cu, Cu-2M alloys exhibit higher impedance values, indicating that the passive layer formed on the surface of Cu-2Ti and Cu-2Zr alloys possesses better corrosion protection characteristics than the one formed on unalloyed Cu.

Based on the impedance responses of unalloyed Cu and Cu-2M alloys, an appropriate equivalent circuit was proposed as shown in Figure 6. Experimental EIS data were best fitted using proposed equivalent circuit. The accuracy of fitting results, shown as solid lines in Figures 4 and 5, was evaluated by the chi-squared (χ^2) values, which were in the order of 10^{-4} for all samples. The equivalent circuit includes the solution resistance, R_s, in series with two RC (time constant), $\tau = R \cdot \mathrm{CPE}$, representing the passive layer and the faradaic charge transfer process. The resistance R_f and constant phase element Q_f correspond to the passive layer, whereas the elements R_{ct} and Q_{dl} can be attributed to the passive layer/electrolyte interface in which R_{ct} is the charge transfer resistance and Q_{dl} represents the double layer capacitance. A constant phase element (CPE), defined as Q, is

introduced in the equivalent circuit instead of a pure capacitance. The origins of the CPE were summarized by Jorcin et al [9], which includes distributed surface roughness and heterogeneity, electrode porosity, slow adsorption reactions, non-uniform potential and current distribution. The impedance of CPE is expressed by:

$$Q = Z_{CPE} = \frac{1}{Y_0(j\omega)^n} \quad (1)$$

where Y_0 is admittance of the electrochemical system, j is the square root of -1, ω is the angular frequency ($\omega = 2\pi f$) and the exponent n is the frequency dispersion factor that depending on its value, CPE can represent pure resistance when $n = 0$, pure capacitance when $n = 1$, inductance when $n = -1$, or Warburg impedance when $n = 0.5$ [10].

It can be seen in Figure 7 that the passive film resistance, R_f, increase with increasing exposure time to the aggressive environment, suggesting that the surface layer becomes more protective with increasing exposure time for all specimens. High passive film resistance can block both the anodic and cathodic reactions. Therefore, the passive layer develops an effective barrier against corrosion. Cu-2M alloys exhibit higher R_f values as compared to unalloyed Cu. This behavior indicates improved barrier properties of the layer present at the surface of Cu-2Zr and Cu-2Ti alloys, which effectively reduces the corrosion progress of metallic substrate. On the other hand, the passive layer capacitance, C_f, progressively decreases for all tested materials with increasing exposure time to the aggressive environment, as shown in Figure 8. The C_f values were derived from CPE parameters using the following equation [11]:

$$C_f = (R_f^{1-n} Q_f)^{1/n} \quad (2)$$

By considering the passive layer to act as a parallel plate dielectric, the capacitance will be related to the thickness according to:

$$C_f = \frac{\varepsilon \varepsilon_0 A}{d} \quad (3)$$

where ε is the dielectric constant of the passive layer, ε_0 the dielectric permittivity of vacuum, A the geometric area, and d is the thickness. Therefore, the lower C_f values exhibited by Cu-2Ti

and Cu-2Zr alloys as compared to unalloyed Cu (Fig. 8) can be related to an increase of the passive layer thickness or a change of passive layer composition.

Figure 9 reports, for unalloyed Cu and Cu-2M alloys, the variation of polarization resistance, R_p, as a function of exposure time to the aggressive environment. In all cases it can be seen that the polarization resistance increases with increasing exposure time, indicating an improvement of corrosion behaviour. Cu-2Zr alloy exhibits higher values of R_p, which is the sum of R_{ct} and R_f [12], as compared to Cu-2Ti alloy and unalloyed Cu. The corrosion rate is inversely related to R_p – the higher the value of R_p the higher the corrosion resistance (lesser corrosion rate). Therefore, the larger R_p values showed by Cu-2Zr alloy with respect to Cu-2Ti one and unalloyed Cu highlight its higher stability in 3.5 *wt.*% NaCl solution.

Figure 10 shows the surface morphology of unalloyed Cu after 168 h exposure to aerated 3.5 *wt.*% NaCl solution. A layer of corrosion products covering the surface of sample can be observed. Electron probe microanalysis revealed that this surface layer is mainly constituted by copper, oxygen and chlorine, as reported in Table 2. It is generally accepted that the corrosion of copper in naturally aerated neutral NaCl solutions involves the cathodic reaction of oxygen according to [13 – 15]:

$$2\ H_2O + O_2 + 4e^- \rightarrow 4\ OH^- \quad (4)$$

The anodic dissolution of copper in the presence of complexing ions such as Cl^- proceeds via a two-step reaction mechanism as follows [16 – 18]:

$$Cu + Cl^- \rightarrow CuCl + e^- \quad (5)$$

$$CuCl + Cl^- \rightarrow CuCl_2^- \quad (6)$$

$$Cu + 2\ Cl^- \rightarrow CuCl_2^- + e^- \quad (7)$$

in the first step, CuCl is formed as an insoluble product, and can be easily adsorbed at the surface electrode. In the next step, the soluble $CuCl_2^-$ is formed from the dissolution of the adsorbed CuCl products (reaction (6)) or of copper itself (reaction (7)).

It was suggested that the presence of $CuCl_2^-$ at the metal surface leads to a hydrolysis reaction and the formation of a passive Cu_2O layer according to [17, 18]:

$$2\ CuCl_2^- + H_2O \rightarrow Cu_2O + 4\ Cl^- + 2\ H^+ \quad (8)$$

Accordingly, on the basis of EPMA results is reasonable to conclude that the passive layer formed at the surface of unalloyed Cu predominantly consists of cuprous chloride and cuprous oxide.

SEM-EPMA characterization of Cu-2Ti and Cu-Zr alloys surface after 168 h exposure to aerated 3.5 *wt.*% NaCl solution revealed a different morphology of the corrosion products layer covering the surface of specimens, as reported in Figure 11. This surface layer is characterized by a significant amount of Ti or Zr, as evidenced by electron probe microanalysis (Tables 3 and 4). Moreover, the oxygen content is relatively high and chlorine significantly low when compared to unalloyed Cu (Table 2).

The composition and morphology of passive layer play an important role in determining the corrosion behaviour of investigated alloys. The different solid corrosion products, formed on their surface at the onset of dissolution, may hinder the transportation of the corrosion medium as well as the mass exchange of reagents. In the present study, Cu-2Ti and Cu-2Zr alloys exhibit a two-phase microstructure characterized by the presence of Cu_4Ti and Cu_9Zr_2 intermetallic compounds (Figs. 1 and 2). The anodic dissolution of these intermetallic phases enables the formation of a Ti- or Zr-enriched passive layer with enhanced protective properties compared to that present at the surface of unalloyed Cu.

During the copper corrosion, the increase of the local pH on copper surface because of the oxygen reduction leads to the precipitation of Ti(IV) and Zr(IV) oxide, according to the E-pH diagrams of titanium and zirconium in water [19]. Titanium or zirconium cations formed during anodic dissolution of Cu_4Ti or Cu_9Zr_2 intermetallic compounds (reaction (9)) react with the hydroxyl ions (reaction (4)) giving rise to the precipitation of TiO_2 or ZrO_2 (reaction (10)):

$$Ti\ (Zr) \rightarrow Ti^{4+}\ (Zr^{4+}) + 4\ e^- \quad (9)$$

$$2\ H_2O + O_2 + 4\ e^- \rightarrow 4\ OH^- \quad (4)$$

$$Ti^{4+}\ (Zr^{4+}) + 4\ OH^- \rightarrow TiO_2\ (ZrO_2) + 2\ H_2O \quad (10)$$

The presence of Ti or Zr oxide layer may explain the differences between the surface morphology of unalloyed Cu (Fig. 10), on one hand, and that of Cu-2M alloys, on the other, evidenced by SEM observations (Fig. 11).

Data reported in this study show that Cu-2M alloy exhibits higher corrosion stability in sodium chloride solution as compared to unalloyed Cu. As a consequence, the obtained electrochemical results lead to the conclusion that the presence of Ti or Zr in the passive layer significantly enhances its protective capabilities. This surface layer hinders the mass exchange of reagents and products between the substrate and the corrosive medium, thus decreasing the corrosion activity and consequently increasing the corrosion resistance. The insulating character of ZrO_2 [20] may contribute to enhance the dielectric properties of the passive layer, thus reinforcing its barrier properties as observed for the "lanthanide-doped" cuprous oxide [21]. This would explain the better corrosion behaviour of Cu-2Zr alloy compared to Cu-2Ti one.

Further investigation is planned aiming at a deeper understanding of the protective behaviour of these surface layers.

4. Conclusions

The corrosion behaviour of Cu-2Ti and Cu-1Zr alloys has been assessed and compared with that of unalloyed Cu. The following conclusions can be drawn:

1. Results from EIS measurements of samples exposed to 3.5 *wt.*% NaCl solution revealed that Cu-2Ti and Cu-2Zr alloys possess significantly improved corrosion resistance in comparison to unalloyed Cu.
2. The increased corrosion stability of Cu-2Ti and Cu-2Zr alloys is ascribed to the formation of a Ti- or Zr-doped passive layer which exhibits enhanced protective properties with respect to that formed on unalloyed Cu (larger R_f values).
3. EPMA characterization of the layer present at the surface of Cu-2Ti and Cu-2Zr alloys evidenced a significant amount of titanium or zirconium in the form of TiO_2 or ZrO_2. As a

consequence of their dissolution, the $CuTi_4$ and Cu_9Zr_2 intermetallic phases act as tanks of titanium and zirconium used to reinforce the passive layer on copper.

4. The better corrosion behaviour of Cu-2Zr alloy compared to Cu-2Ti one (larger R_p values) is ascribed to the insulating character of zirconium oxide which may contribute to enhance the dielectric properties of the passive layer. Accordingly, this surface layer shows improved barrier properties thereby exerting an effective inhibiting action towards the corrosion process.

5. References

[1] W.A. Soffa, D.E. Laughlin, *Prog. Mater. Sci.* **2004**;49:347

[2] M. Metikos-Hukovic, R. Babic, I. Paic, *J. Appl. Electrochem.* **2000**;30:617

[3] Y. Feng, K.S. Siow, W.K. Teo, K.L. Tan, A.K. Hseih, *Corrosion* **1997**;53:389

[4] H. Wey, L.-f. Hou, Y.-c. Cui, Y.-h. Wei, *Trans. Nonferrous Met. Soc. China* **2018**;28:669

[5] H.B. Lu, Y. Li, F.H. Wang, *Electrochim. Acta* **2006**;52:474

[6] K. Rahmouni, M. Keddam, A. Srhiri, H. Takenouti, *Corros. Sci.* **2005**;47:3249

[7] Y. Van Ingelgem, H. Hubin, J. Vereecken, *Electrochim. Acta* **2007**;52:7642

[8] A. Drach, L. Tsukrov, J. De Cew, J. Aufrecht, A. Grohbauer, U. Hofmann, *Corros. Sci.* **2013**;76:453

[9] J.-B. Jorcin, M.E. Orazem. N. Pebere, B. Tribollet, *Electrochim. Acta* **2006**;51:1473

[10] U. Rammelt, G. Reinhard, *Electrochim. Acta* **1990**;35:1049

[11] J.R. Macdonald, *Impedance Spectroscopy*, **1987**, J Wiley & Sons, New York

[12] J.R. Scully, *Corrosion* **2000**;56:199

[13] M. Vasquez, S.R. de Sanchez, E.J. Calvoy, D. Schiffrin, *J. Electroanal. Chem.* **1994**;374:189

[14] S. Cere, M. Vasquez, S.R. de Sanchez, D. Schiffrin, *J. Electroanal. Chem.* **2001**;505:118

[15] R. Procaccini, D. Schiffrin, *J. Appl. Electrochem.* **2009**;39:177

[16] P. Sury, H.R. Otswald, *Corros. Sci.* **1972**;12:77

[17] A.I. Bacarella, J.C. Griess, *J. Electrochem. Soc.* **1973**;120:459

[18] G. Kear, B.D. Barker, K. Stokes, F.C. Walsh, *J. Appl. Electrochem.* **2004**;34:659

[19] M. Pourbaix, *Atlas of electrochemical equilibria in aqueous solutions*, **1974**, NACE Cebelcorr, Houston

[20] P. Meisterjahn, H.W. Hoppe, J.W. Schultze, *J. Electroanal. Chem.* **1987**:217;159

[21] F. Rosalbino, R. Carlini, F. Soggia, G. Zanicchi, G. Scavino, *Corros. Sci.* **2012**;58:139

Figure captions

Figure 1 – Optical micrograph of Cu-2Ti alloy (Nital etching). Cu solid solution (bright-grey phase) and Cu_4Ti intermetallic compound (dark-grey phase).

Figure 2 – Optical micrograph of Cu-2Zr alloy (Nital etching). Cu solid solution (dark-grey phase) and Cu_9Zr_2 intermetallic compound (bright-grey phase).

Figure 3 – Open circuit potential vs. time profile for unalloyed Cu and Cu-2M alloys after 1 h exposure to naturally aerated 3.5 *wt.*% NaCl solution

Figure 4 – Representative Nyquist diagrams of unalloyed Cu for various exposure times to naturally aerated 3.5 *wt.*% NaCl solution

Figure 5 – Representative Nyquist diagrams of: (a) Cu-2Ti and (b) Cu-2Zr alloys for various exposure times to naturally aerated 3.5 *wt.*% NaCl solution

Figure 6 - Equivalent electrical circuit used for EIS modeling

Figure 7 – Passive layer resistance, R_f, for unalloyed Cu and Cu-2M alloys as a function of exposure time to naturally aerated 3.5 *wt.*% NaCl

Figure 8 – Passive layer capacitance, C_f, for unalloyed Cu and Cu-2M alloys as a function of exposure time to naturally aerated 3.5 *wt.*% NaCl

Figure 9 – Polarization resistance, R_p, for unalloyed Cu and Cu-2M alloys as a function of exposure time to naturally aerated 3.5 *wt.*% NaCl

Figure 10 – SEM micrograph of the corrosion products layer formed at the surface of unalloyed Cu after 168 h exposure to naturally aerated 3.5 *wt.*% NaCl solution.

Figure 11 – SEM micrograph of the corrosion products layer formed at the surface of Cu-2M alloys after 168 h exposure to naturally aerated 3.5 *wt.*% NaCl solution. (a) Cu-2Ti alloy; (b) Cu-2Zr alloy

Table 1 – SEM-EPMA data on Cu-2M alloys

Alloy	**Measured composition (*wt.*%)**			**Phases**	**Phase composition (*wt.*%)**		
	Cu	Zr	Ti		Cu	Zr	Ti
Cu-2Ti	98.01	0.00	1.99	(Cu)	99.90	0.00	0.10
				Cu_4Ti	84.14		15.86
Cu-2Zr	98.01	1.99	0.00	(Cu)	99.94	0.06	0.00
				Cu_9Zr_2	75.82	24.18	

Table 2 - Electron probe microanalysis of the corrosion products present at the surface of unalloyed Cu after 168 h exposure to naturally aerated 3.5 *wt.*% NaCl solution

Elements	**O**	**Cl**	**Cu**
wt.%	20.29	10.57	69.14

Table 3 – Electron probe microanalysis of the corrosion products present at the surface of Cu-2Ti alloy after 168 h exposure to naturally aerated 3.5 wt.% NaCl solution

Elements	**O**	**Cl**	**Ti**	**Cu**
Mass%	30.35	2.40	11.53	55.72

Table 4 – Electron probe microanalysis of the corrosion products present at the surface of Cu-2Zr alloy after 168 h exposure to naturally aerated 3.5 *wt.*% NaCl solution

Elements	**O**	**Cl**	**Zr**	**Cu**
Mass%	30.53	1.84	12.01	55.62

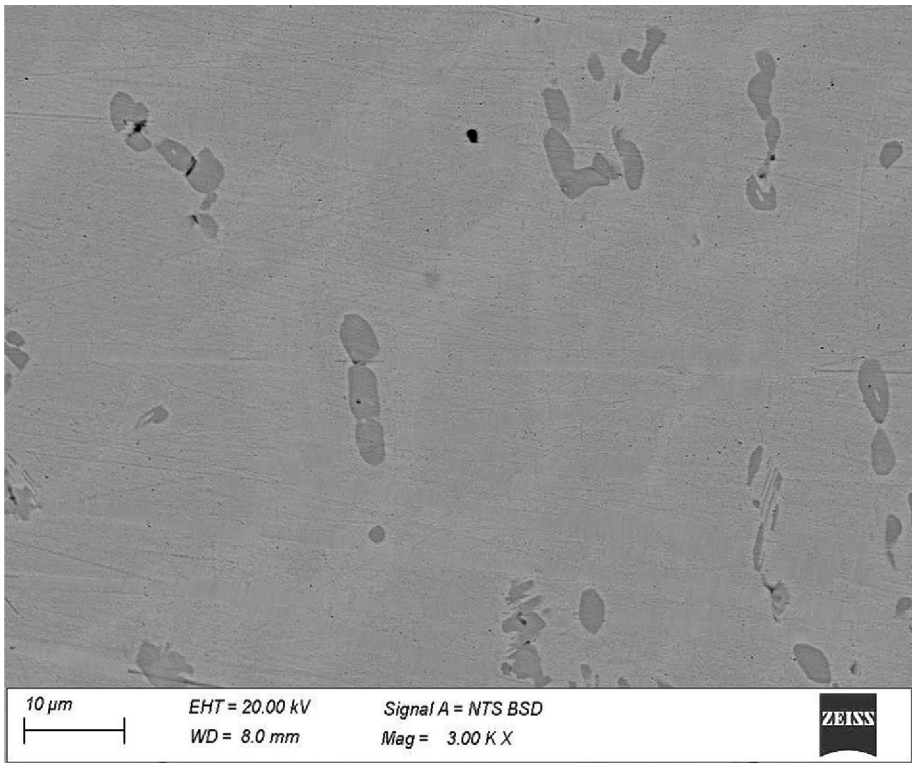

Figure 1

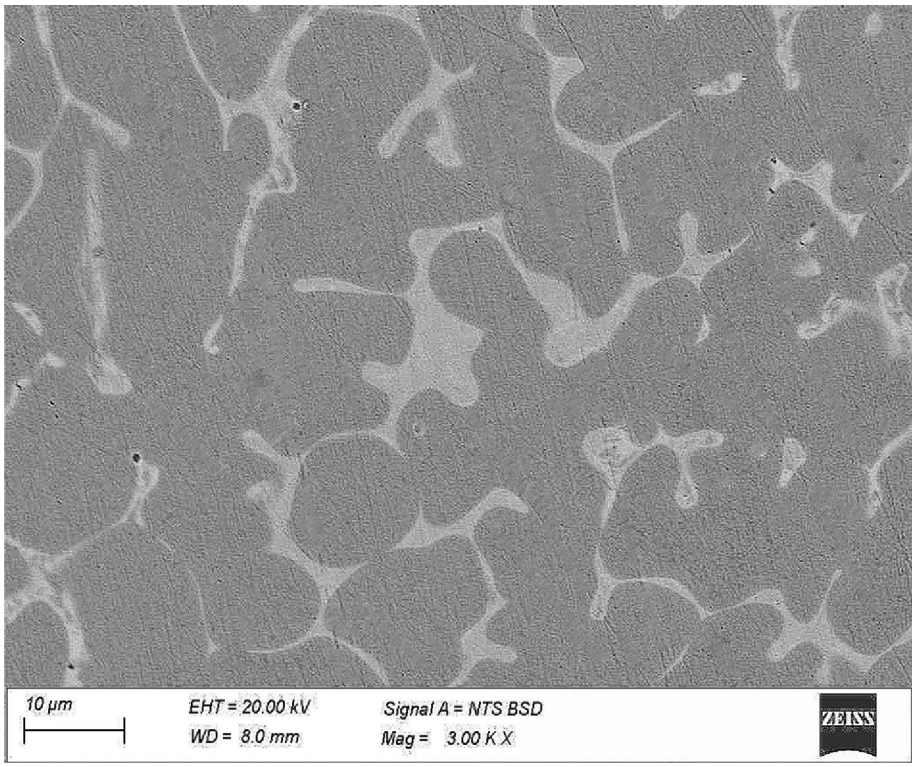

Figure 2

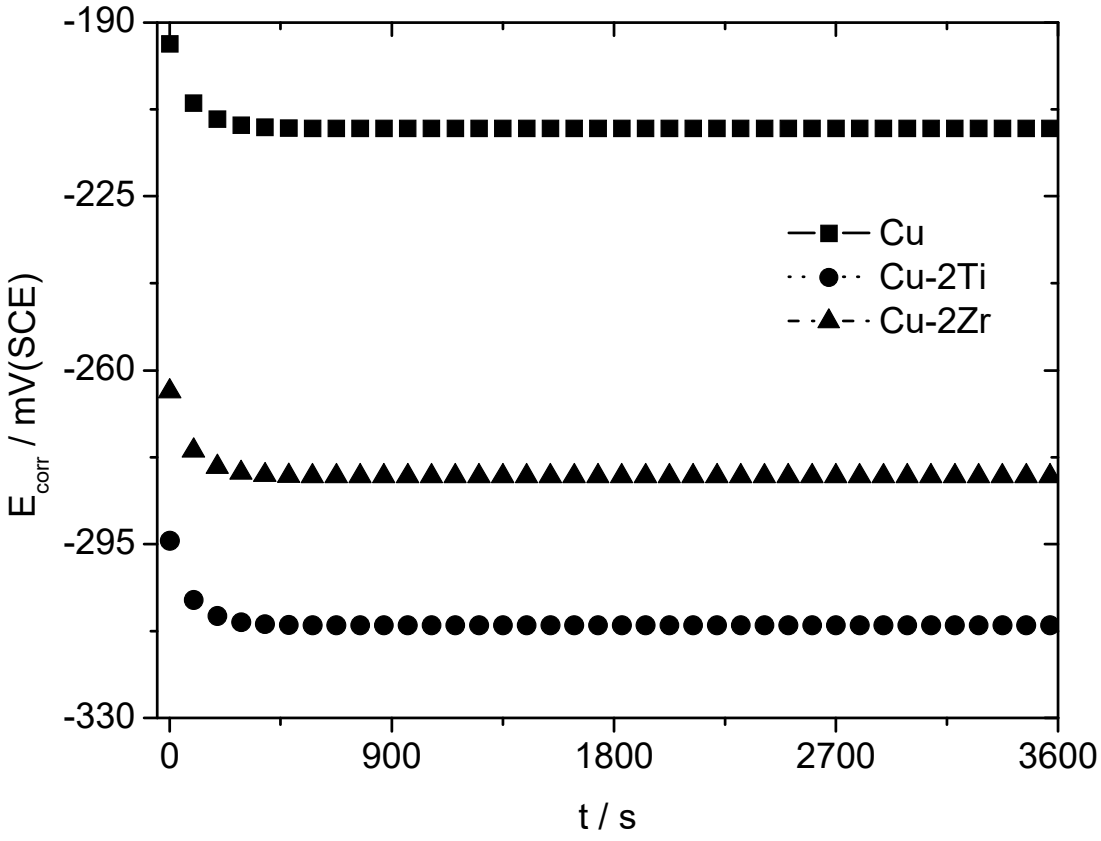
-190
-225
-260
-295
-330
0
900
1800
2700
3600
t / s
E_corr / mV(SCE)
Cu
Cu-2Ti
Cu-2Zr

Figure 3

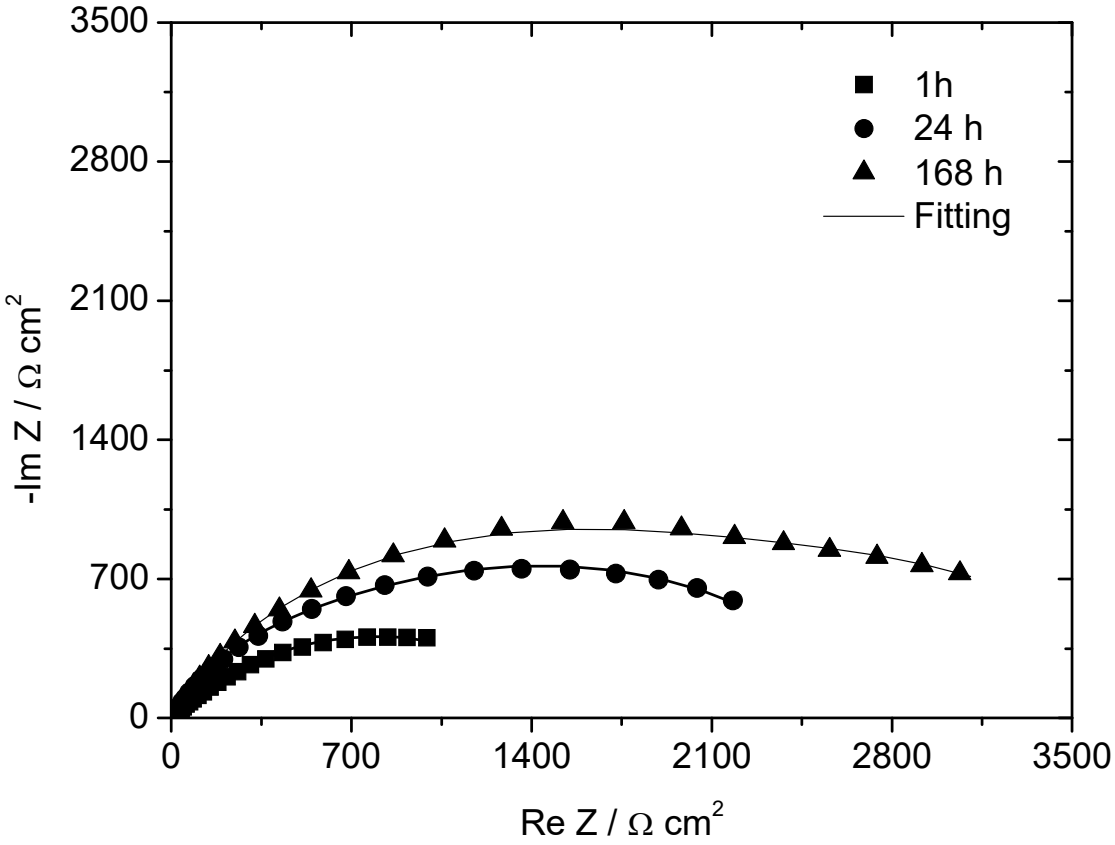
3500
2800
2100
1400
700
0
0
700
1400
2100
2800
3500
-Im Z / Ω cm2
Re Z / Ω cm2
1h
24 h
168 h
Fitting

Figure 4

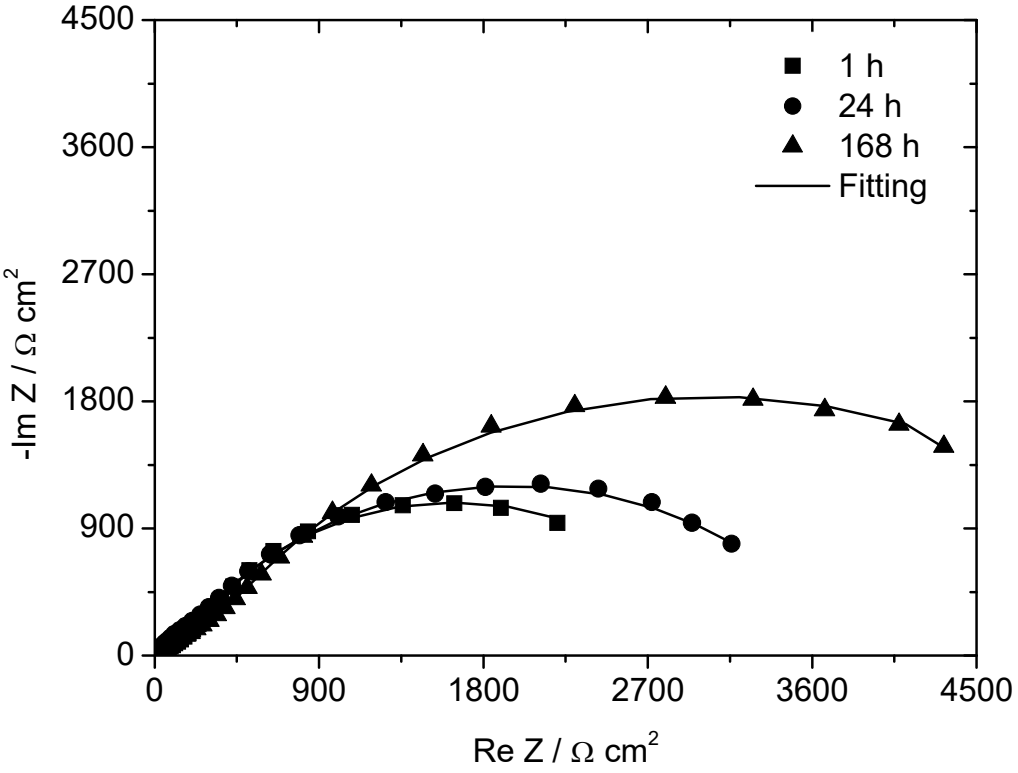
4500
3600
2700
1800
900
0
0
900
1800
2700
3600
4500
-Im Z / Ω cm2
Re Z / Ω cm2
1 h
24 h
168 h
Fitting

(a)

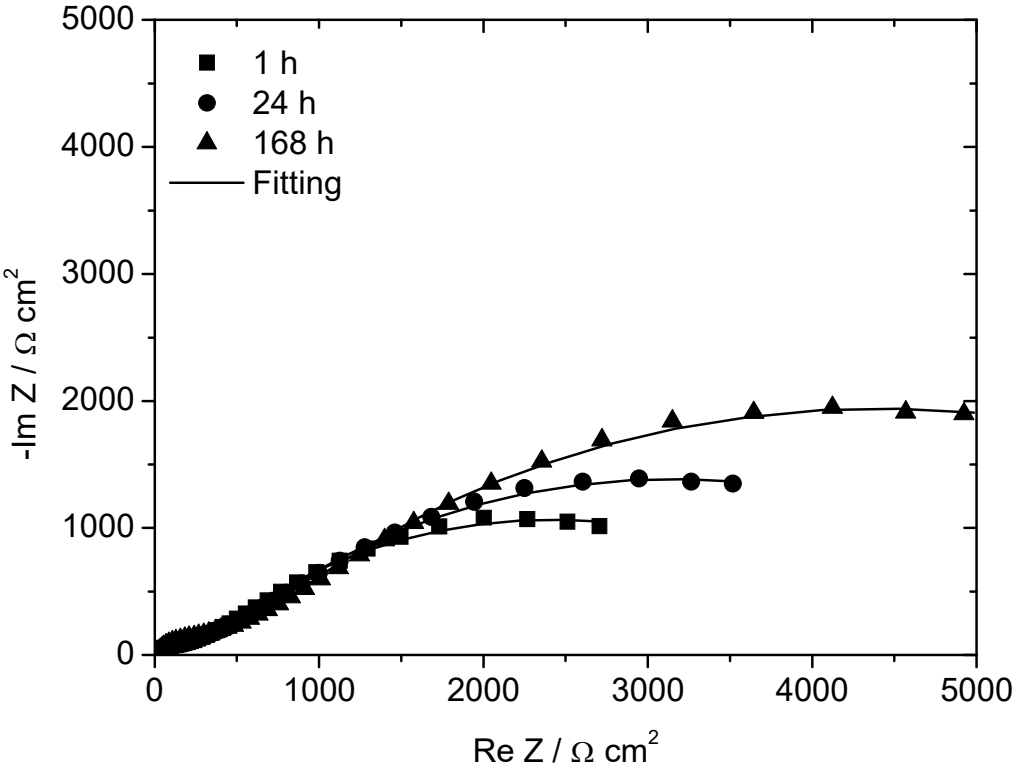
5000
4000
3000
2000
1000
0
0
1000
2000
3000
4000
5000
-Im Z / Ω cm2
Re Z / Ω cm2
1 h
24 h
168 h
Fitting

(b)

Figure 5

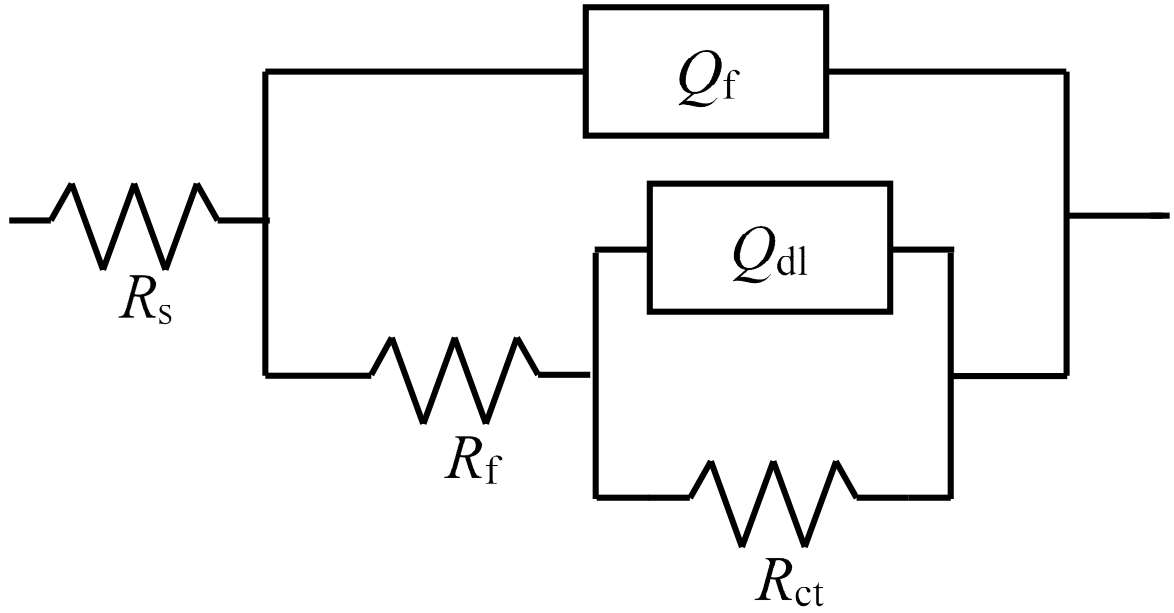

Figure 6

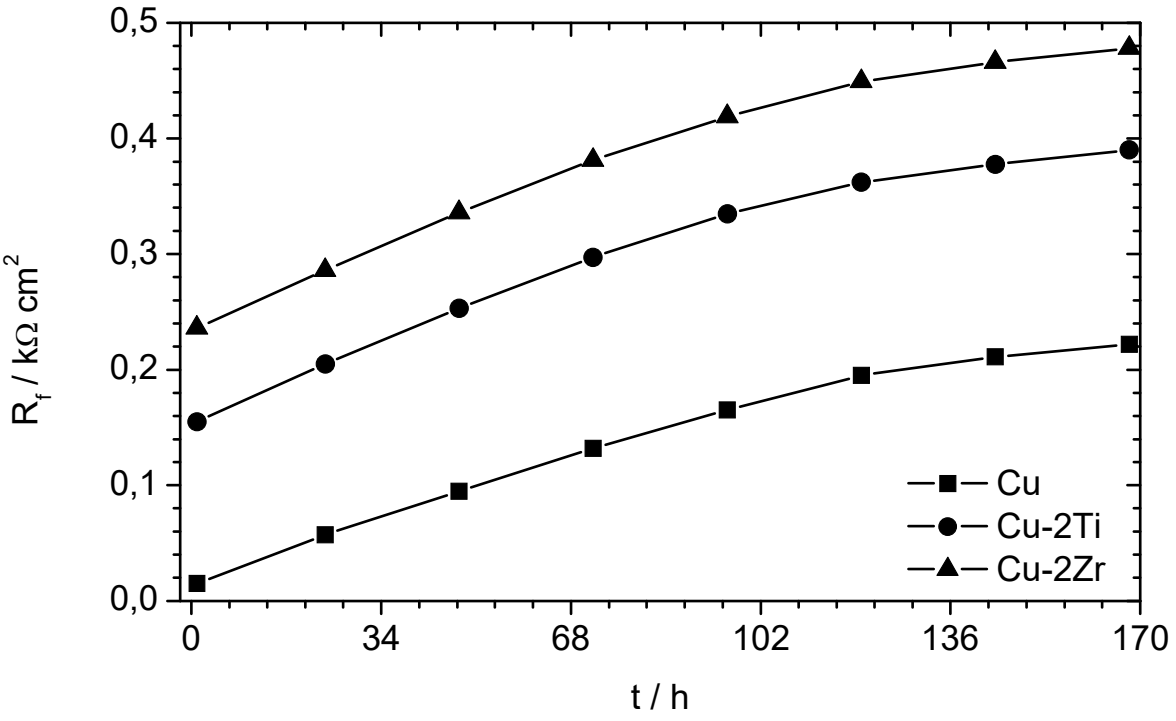

Figure 7

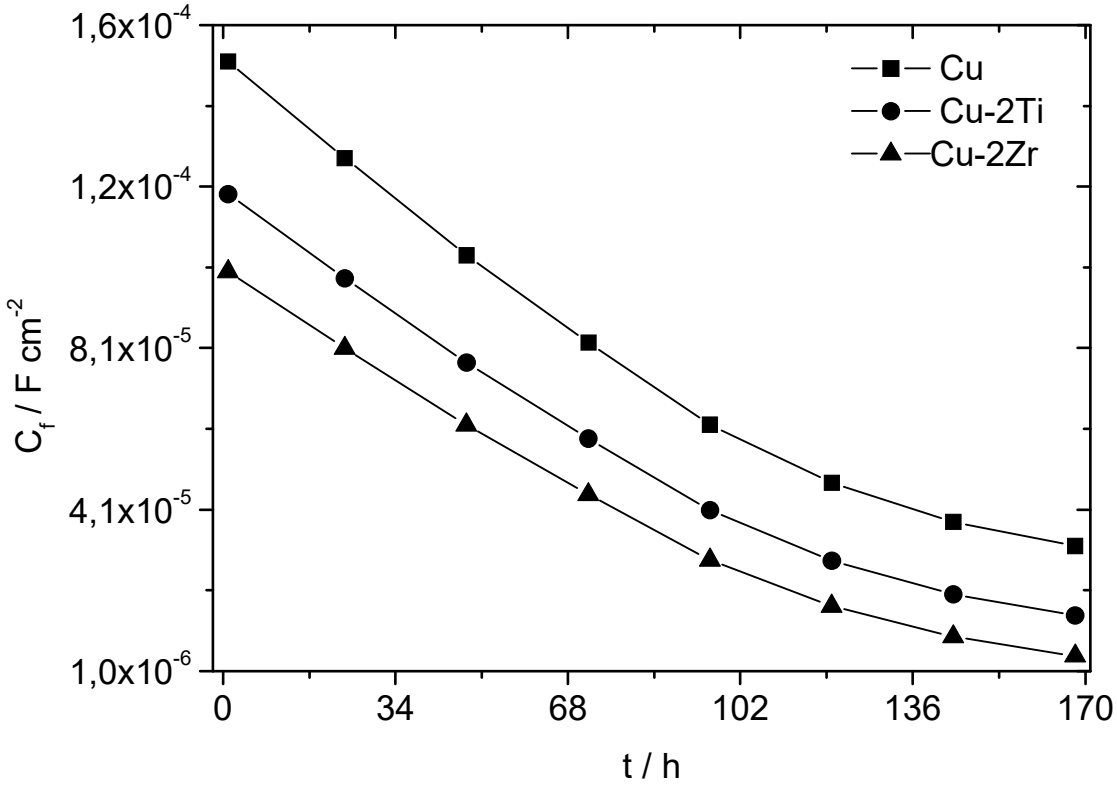
1,6x10-4
1,2x10-4
8,1x10-5
4,1x10-5
1,0x10-6
Cf / F cm-2
0
34
68
102
136
170
t / h
Cu
Cu-2Ti
Cu-2Zr

Figure 8

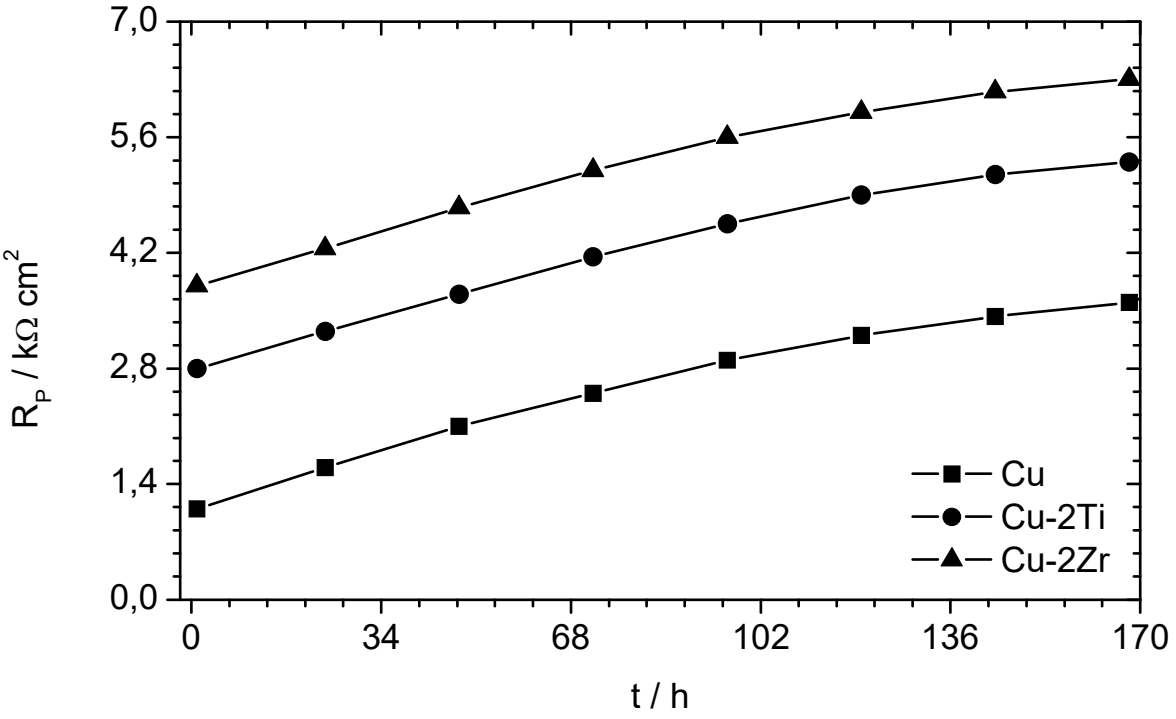

Figure 9

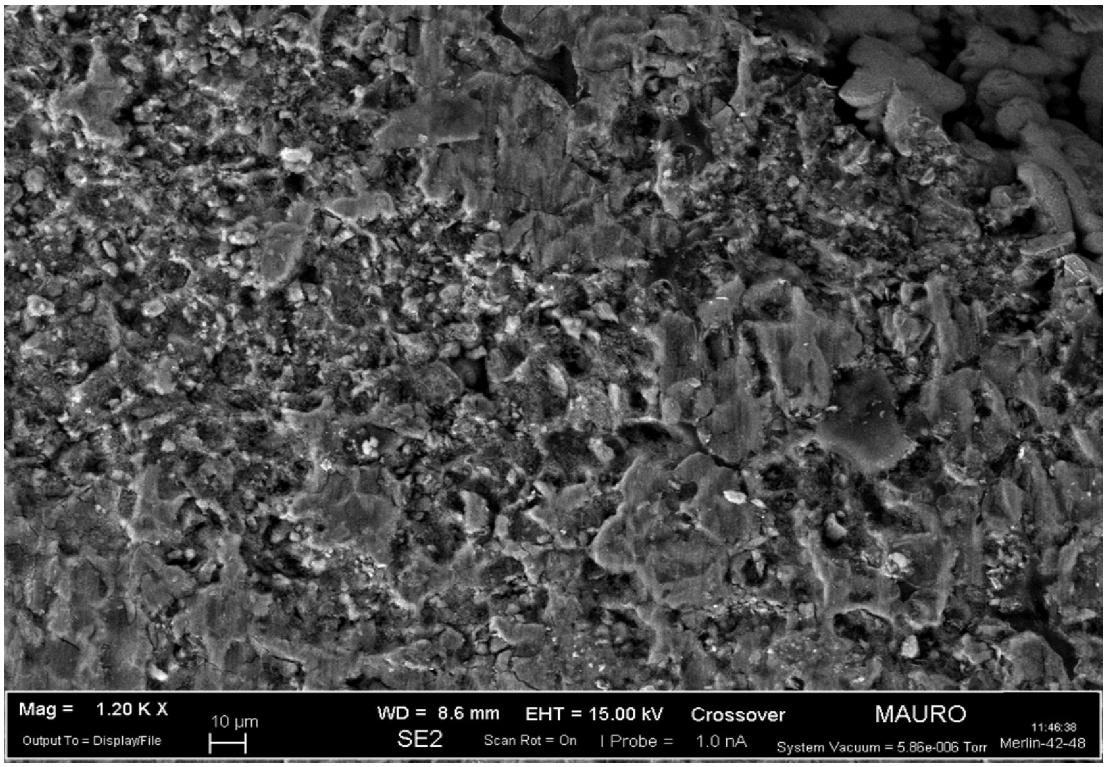
Mag = 1.20 K X
Output To = Display/File
10 µm
WD = 8.6 mm
SE2
EHT = 15.00 kV
Scan Rot = On
Crossover
I Probe = 1.0 nA
MAURO
System Vacuum = 5.86e-006 Torr
11:46:38
Merlin-42-48

Figure 10

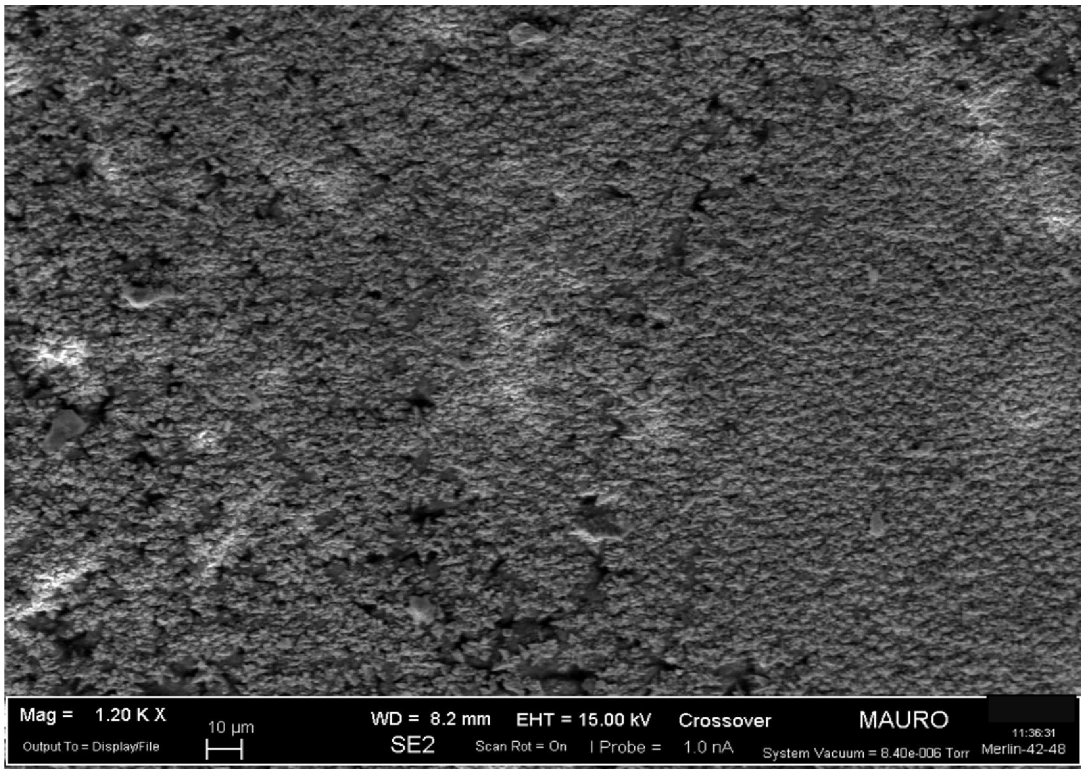
Mag = 1.20 K X
10 µm
WD = 8.2 mm EHT = 15.00 kV Crossover MAURO
Output To = Display/File
SE2 Scan Rot = On I Probe = 1.0 nA
System Vacuum = 8.40e-006 Torr Merlin-42-48
11:36:31

(a)

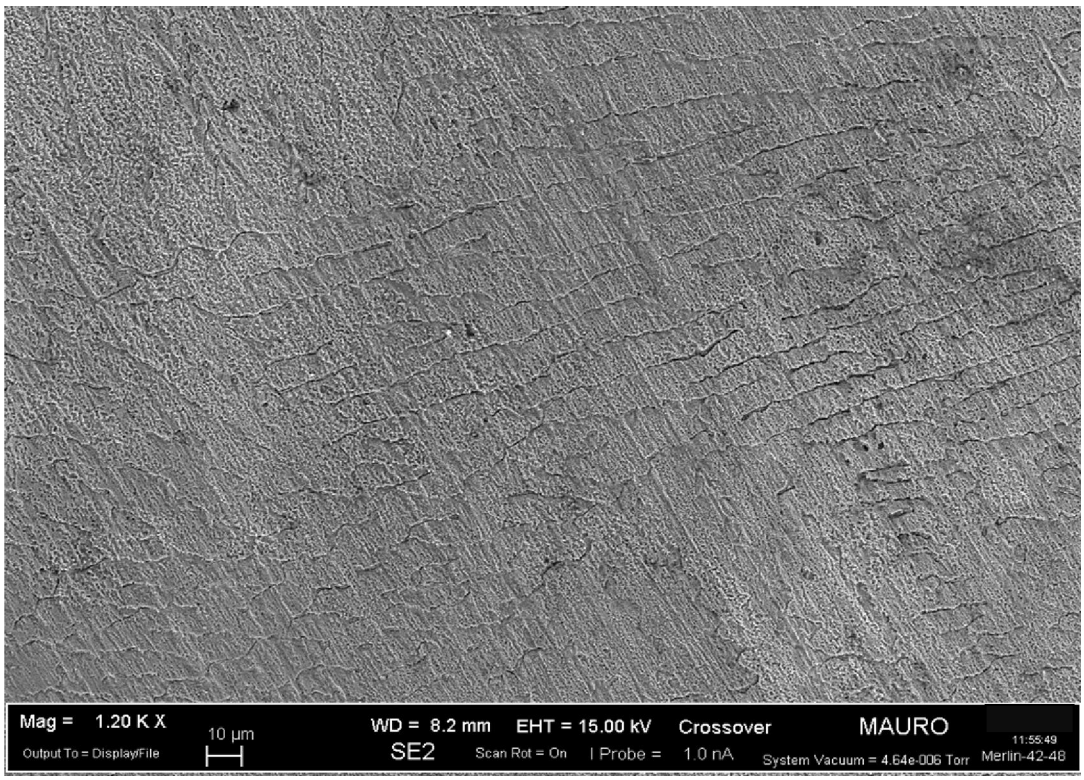
Mag = 1.20 K X
10 µm
WD = 8.2 mm EHT = 15.00 kV Crossover MAURO
Output To = Display/File
SE2 Scan Rot = On I Probe = 1.0 nA
System Vacuum = 4.64e-006 Torr Merlin-42-48
11:55:49

(b)

Figure 11